INTERNATIONAL JOURNAL FOR NUMERICAL METHODS IN FLUIDS
Int. J. Numer. Meth. Fluids **30**: 713–724 (1999)

SPECTRAL METHODS FOR THE SIMULATION OF INCOMPRESSIBLE FLOWS IN SPHERICAL SHELLS

A. TILGNER*

Institute of Physics, University of Bayreuth, 95440 Bayreuth, Germany

SUMMARY

A spatial discretization of the incompressible Navier–Stokes equation is presented in which the velocity is decomposed using poloidal and toroidal scalars whose spatial dependence is given in terms of spherical harmonics and Chebychev polynomials. The radial resolution needs to be large enough at any given angular resolution in order to avoid instability in the simulation of rotating flows. Several semi-implicit time steps are discussed. The most accurate scheme is an integrating factor technique. Copyright © 1999 John Wiley & Sons, Ltd.

KEY WORDS: spectral methods; implicit time steps; rotating fluids; precession

1. INTRODUCTION

Flow problems in spherical geometry are of central importance for geo- and astrophysics. Attention has mostly focused on convection in stars, planetary atmospheres and the earth's mantle. The generation of the earth's magnetic field by fluid motion in the earth's core has also been greatly studied recently. In most problems of interest rotation plays a major role and the appropriate geometry is that of a spherical shell rather than a full sphere.

The solver presented here uses spectral decompositions. Spectral methods [1] provide high precision when dealing with stability or transition problems and generally require fewer grid points at equal accuracy compared with local methods. In addition, the basis functions may be good approximations to the actual solution so that a relatively small number of modes can be enough for accurate computation. The savings compared with a local grid method are particularly striking in the case of precession-driven flows discussed below. In spherical geometry, spherical harmonics are usually chosen to discretize the angular variables. This system of functions automatically handles a co-ordinate singularity and avoids the crowding of grid points near the poles, which plagues straightforward finite difference discretization, thus permitting larger time steps in time integrations [2]. The use of spherical harmonics also greatly simplifies the treatment of non-local boundary conditions that arise at a spherical conductor–vacuum interface in magneto-hydrodynamic problems.

One of the first complete descriptions of a spectral code using spherical harmonics was given by Young [3]. The radial direction was treated with a Green's function method implicitly assuming a finite difference discretization in radius. The method simulates convection in the framework of the Boussinesq approximation. Glatzmaier [4] later presented a method to solve

* Correspondence to: Universitat Bayreuth, Physikalisches Institut 4, D-95440 Bayreuth, Germany.

CCC 0271–2091/99/140713–12$17.50

Received December 1997
Revised August 1998

for compressible convection flows within the anelastic approximation. Radial discretization was performed with a Chebychev collocation method and the computation of the non-linear terms was improved. Both authors used a poloidal–toroidal decomposition [5] for solenoidal vector fields. More recently, a different formal approach to spatial discretization utilizing vector spherical harmonics has been described by Dumas and Leonard [6].

The present paper reports on a spectral code using poloidal–toroidal decompositions for incompressible flows. Special attention is paid to the case of fast rotation. Experience has been gathered by applying the method to convection [7,8], the kinematic [9] and full dynamo problems and precession driven flows [10]. This last problem is conceptually the simplest but turned out to be computationally the most demanding. In order to keep formulas short yet readily extendible to other problems, the actual discretizations will be given for the precession problem only. The main emphasis of the paper is on accurate time stepping methods.

Section 2 presents the spatial discretization with a special discussion of the Coriolis term. Section 3 deals with time stepping methods. Usual semi-implicit time steps are compared with the integrating factor technique. Section 4 shows sample runs and conclusions.

2. SPATIAL DISCRETIZATION

Consider an incompressible fluid of density ρ and kinematic viscosity ν in a spherical shell of gap width d, rotating with angular frequency ω about the z-axis. Units of length and time are chosen as d and $1/\omega$ respectively. If the shell furthermore executes precessional motion characterized by the precession vector $\omega\boldsymbol{\Omega}$, the non-dimensional equations for the velocity $\boldsymbol{u}(\boldsymbol{r}, t)$ read in a frame of reference attached to the precessing casing [11,12]:

$$\frac{\partial}{\partial t}\boldsymbol{u} + (\nabla \times \boldsymbol{u}) \times \boldsymbol{u} + 2(\hat{\boldsymbol{z}} + \boldsymbol{\Omega}) \times \boldsymbol{u} = -\nabla\phi + E\nabla^2\boldsymbol{u} - (\boldsymbol{\Omega} \times \hat{\boldsymbol{z}}) \times \boldsymbol{r}, \tag{1}$$

$$\nabla \cdot \boldsymbol{u} = 0. \tag{2}$$

Hats denote unit vectors. The Ekman number E is given by $E = \nu/d^2\omega$. ϕ stands for a reduced pressure that is immaterial in the sequel because only the curl of (1) will be used. The precession axis $\hat{\boldsymbol{\Omega}}$ forms the angle α ($0 < \alpha < \pi/2$) with the z-axis and is time-dependent in the chosen system of reference:

$$\hat{\boldsymbol{\Omega}} = \sin\alpha \cos t\, \hat{\boldsymbol{x}} - \sin\alpha \sin t\, \hat{\boldsymbol{y}} + \cos\alpha\, \hat{\boldsymbol{z}}. \tag{3}$$

The boundary conditions require that $\boldsymbol{u} = 0$ at $r = r_\mathrm{i}$, r_o, where r_i and r_o denote the inner and outer radii of the shell. Due to the choice of units, $r_\mathrm{o} - r_\mathrm{i} = 1$.

The solenoidal velocity field can be written in terms of poloidal and toroidal scalars Φ and Ψ:

$$\boldsymbol{u} = \nabla \times \nabla \times (\Phi\hat{\boldsymbol{r}}) + \nabla \times (\Psi\hat{\boldsymbol{r}}), \tag{4}$$

which are themselves decomposed into radial and angular parts:

$$\Phi = r \sum_{l=1}^{\infty} \sum_{m=-l}^{l} V_l^m(r, t) P_l^m(\cos\theta)\, \mathrm{e}^{\mathrm{i}m\varphi}, \qquad \Psi = r^2 \sum_{l=1}^{\infty} \sum_{m=-l}^{l} W_l^m(r, t) P_l^m(\cos\theta)\, \mathrm{e}^{\mathrm{i}m\varphi}, \tag{5}$$

in spherical polars (r, θ, φ). $P_l^m(\cos\theta)$ denotes the associated Legendre functions. The factors r and r^2 in (5) are not essential but convenient because they reduce the variation of V_l^m and W_l^m with r in most problems. Operating with $\hat{\boldsymbol{r}} \cdot \nabla \times$ and $\hat{\boldsymbol{r}} \cdot \nabla \times \nabla \times$ on (1) one obtains:

$$\frac{\partial}{\partial t}\mathscr{D}_l V_l^m - E\cdot\mathscr{D}_l^2 V_l^m = \frac{r}{l(l+1)}[\hat{\boldsymbol{r}}\cdot\nabla\times\nabla\times\{\boldsymbol{\Omega}'\times\boldsymbol{u}\}]_l^m, \tag{6a}$$

$$\frac{\partial}{\partial t}W_l^m - E\left(\frac{\partial^2}{\partial r^2}+\frac{4}{r}\frac{\partial}{\partial r}+\frac{2-l(l+1)}{r^2}\right)W_l^m = -\frac{1}{l(l+1)}[\hat{\boldsymbol{r}}\cdot\nabla\times\{\boldsymbol{\Omega}'\times\boldsymbol{u}\}]_l^m + [f]_l^m, \tag{6b}$$

with

$$\boldsymbol{\Omega}' = \nabla\times\boldsymbol{u} + 2(\hat{\boldsymbol{z}}+\boldsymbol{\Omega}), \qquad \mathscr{D}_l = \frac{\partial^2}{\partial r^2}+\frac{2}{r}\frac{\partial}{\partial r}-\frac{l(l+1)}{r^2}$$

and

$$f = \Omega\sin\alpha[iP_1^1\,\mathrm{e}^{i(\varphi+t)} + 2iP_1^{-1}\,\mathrm{e}^{-i(\varphi+t)}], \qquad \boldsymbol{\Omega} = \Omega\hat{\boldsymbol{\Omega}}.$$

$[\ ]_l^m$ denotes the l,m-component of the quantity in the square bracket. These equations need to be solved subject to the boundary conditions

$$V_l^m = \frac{\partial V_l^m}{\partial r} = W_l^m = 0 \quad \text{at } r = r_\mathrm{i}, r_\mathrm{o}. \tag{7}$$

Because Φ and Ψ are real, $V_l^{m*} = V_l^{-m}$ and $W_l^{m*} = W_l^{-m}$, so that only components with $m \geq 0$ need to be stored. Equations (6a) and (6b) are solved with a Chebychev collocation method. The sums in (5) are truncated at L to include only terms with $l \leq L$ and the functions V_l^m and W_l^m are expanded in n_r Chebychev polynomials T_n as

$$V_l^m(r,t) = \sum_{n=0}^{n_r-1} v_{l,n}^m(t)T_n(x), \qquad W_l^m(r,t) = \sum_{n=0}^{n_r-1} w_{l,n}^m(t)T_n(x), \tag{8}$$

with $x = 2(r-r_\mathrm{i})-1$. The collocation points are placed in direct space at $r_n + r_\mathrm{i} + 1/2\{1+\cos[\pi(n-1)/(n_r-1)]\}$, with $n = 1,\ldots,n_r$, so that a fast cosine transform can be used to switch between physical and spectral space. Equations (6) are enforced at every collocation point and the spectral representation in radius is merely used to compute derivatives.

It is very convenient to introduce a radial stretching function at this stage if one wishes to concentrate collocation points in specific regions, e.g. the boundaries. This can be accomplished by leaving the collocation points in x space at $x_n = \cos[\pi(n-1)/(n_r-1)]$, so that fast cosine transforms can still be used, but by changing the x-dependence of r. In order to crowd grid points near the boundaries, a useful class of stretching functions is

$$r = r_\mathrm{i} + \frac{1}{2}\left(\frac{\sin(\beta\pi x/2)}{\sin(\beta\pi/2)}+1\right), \quad 0<\beta<1. \tag{9}$$

The restriction on β ensures invertibility of $r(x)$. $\beta = 0$ recovers the traditional Chebychev collocation points. Very few changes need to be made in the code to incorporate a radial stretching function: The definition of the collocation points is of course modified and the $r(x)$ relationship also enters the computation of derivatives, e.g.

$$\frac{\partial}{\partial r}V_l^m(r,t) = \sum_{n=0}^{n_r-1} v_{l,n}^m(t)\frac{\mathrm{d}}{\mathrm{d}x}T_n(x)\frac{\mathrm{d}x}{\mathrm{d}r},$$

where the derivatives of $T_n(x)$ are computed with recurrence relations.

Evaluation of the right-hand-sides of Equations (6a) and (6b) requires the calculation of the radial component of the curl and the radial component of the curl of the curl of a vector $\boldsymbol{S} = S_r\hat{\boldsymbol{r}} + S_\theta\hat{\boldsymbol{\theta}} + S_\varphi\hat{\boldsymbol{\varphi}}$. The auxiliary quantities $P_r = S_r$, $P_\theta = S_\theta/(r\sin\theta)^{-1}$ and $P_\varphi = S_\varphi/(r\sin\theta)^{-1}$ are computed in direct space and then transformed into r,l,m-space. The desired derivatives are now easily obtained:

$$[\hat{\boldsymbol{r}}\cdot\nabla\times\boldsymbol{S}]_l^m=(l+1)\frac{l-m}{2l-1}[P_\varphi]_{l-1}^m-l\frac{l+m+1}{2l+3}[P_\varphi]_{l+1}^m-im[P_\theta]_l^m, \tag{10a}$$

$$[\hat{\boldsymbol{r}}\cdot\nabla\times\nabla\times\boldsymbol{S}]_l^m=l(l+1)[P_r]_l^m+\frac{1}{r^2}\frac{\mathrm{d}}{\mathrm{d}r}\left(r^2\left\{(l+1)\frac{l-m}{2l-1}[P_\theta]_{l-1}^m-l\frac{l+m+1}{2l+3}[P_\theta]_{l+1}^m+im[P_\varphi]_l^m\right\}\right). \tag{10b}$$

The computation of the radial derivative in (10b) requires a transform into Chebychev space and back. Due to different normalizations in the basis functions, the coefficients in (10a) and (10b) are simpler than those in the equivalent formulas of Reference [4]. Note that when evaluating (10a) and (10b) at the highest order L retained in the truncation, severe errors may occur because the components of $\boldsymbol{S}$ at order $L+1$ are not known. In the final version of the code, $[\hat{\boldsymbol{r}}\cdot\nabla\times\boldsymbol{S}]_L^m$ and $[\hat{\boldsymbol{r}}\cdot\nabla\times\nabla\times\boldsymbol{S}]_L^m$ were set to zero. The method then became more stable, though not more accurate.

As indicated in (6), the Coriolis force is most conveniently included in the non-linear terms. However, when dealing with linearized equations it is better to compute the Coriolis term directly in order to avoid the time consuming steps required for the calculation of the non-linear terms. The relevant formulas are:

$$\begin{aligned}-\frac{2}{l(l+1)}&[\hat{\boldsymbol{r}}\cdot\nabla\times(\hat{\boldsymbol{z}}\times\boldsymbol{u})]_l^m\\&=\frac{2}{l(l+1)}\frac{1}{r^2}\left\{\frac{l(l+1)(l+2)(l+m+1)}{2l+3}V_{l+1}^m+\frac{l(l+2)(l+m+1)}{2l+3}\left(V_{l+1}^m+r\frac{\partial V_{l+1}^m}{\partial r}\right)\right.\\&\left.-\frac{(l+1)l(l-1)(l-m)}{2l-1}V_{l-1}^m+\frac{(l+1)(l-1)(l-m)}{2l-1}\left(V_{l-1}^m+r\frac{\partial V_{l-1}^m}{\partial r}\right)+im\,r^2W_l^m\right\},\end{aligned} \tag{11a}$$

$$\begin{aligned}\frac{2r}{l(l+1)}&[\hat{\boldsymbol{r}}\cdot\nabla\times\nabla\times(\hat{\boldsymbol{z}}\times\boldsymbol{u})]_l^m=\frac{2}{l(l+1)}\\&\times\left\{-\frac{l(l+1)(l+2)(l+m+1)}{2l+3}W_{l+1}^m-\frac{l(l+2)(l+m+1)}{2l+3}\left(2W_{l+1}^m+r\frac{\partial W_{l+1}^m}{\partial r}\right)\right.\\&\left.+\frac{(l+1)l(l-1)(l-m)}{2l-1}W_{l-1}^m-\frac{(l+1)(l-1)(l-m)}{2l-1}\left(2W_{l-1}^m+r\frac{\partial W_{l-1}^m}{\partial r}\right)+im\,\mathscr{D}_lV_l^m\right\}.\end{aligned} \tag{11b}$$

When writing a new code it is a rewarding consistency check to verify that the same results can be obtained with Equations (10a) and (10b) and (11a) and (11b).

Geo- and astrophysical applications are frequently interested in rapidly rotating systems. In the limit of fast rotation ($E\to 0$) the dissipative term drops from (1) and the kinetic energy of the flow is conserved, $(\partial/\partial t)\int\boldsymbol{u}^2\,\mathrm{d}V=0$. The question arises as to whether the truncated system will also conserve energy. It is well-known [1] that if the basis functions of a Galerkin spectral method are mutually orthogonal in the scalar product, which also occurs in the conservation law, the numerical method will exactly obey the same conservation law. The angular variables are indeed discretized with a Galerkin method, but the radial direction is not. Since the T_n are orthogonal to each other in a scalar product defined with the weight

$(1-x^2)^{-1/2}$, it appears difficult to find a strictly energy conserving method based on Chebychev polynomials. In the present formulation the quality of energy conservation is thus expected to depend on radial resolution. To investigate the issue, the normal mode problem has been considered [12]:

$$p\boldsymbol{u} + 2\hat{\boldsymbol{z}} \times \boldsymbol{u} = -\nabla\phi, \qquad \nabla\cdot\boldsymbol{u} = 0, \qquad \hat{\boldsymbol{r}}\cdot\boldsymbol{u} = 0 \quad \text{at} \quad r = r_\mathrm{i}, r_\mathrm{o}. \tag{12}$$

The eigenvalues p are purely imaginary. The imaginary parts $\mathrm{Im}\{p\}$ correspond to the frequencies of the inertial modes $\boldsymbol{u}$ and lie in the interval $[-2, 2]$. Equation (12) is reformulated in terms of poloidal and toroidal scalars:

$$p\begin{pmatrix} \mathscr{D}_l V_l^m \\ W_l^m \end{pmatrix} = \begin{pmatrix} \dfrac{2r}{l(l+1)}[\hat{\boldsymbol{r}}\cdot\nabla\times\nabla\times\{\hat{\boldsymbol{z}}\times\boldsymbol{u}\}]_l^m \\ -\dfrac{2r}{l(l+1)}[\hat{\boldsymbol{r}}\cdot\nabla\times\{\hat{\boldsymbol{z}}\times\boldsymbol{u}\}]_l^m \end{pmatrix}. \tag{13}$$

The right-hand-side couples in l but decouples in m (see (11a) and (11b)). After discretization, the dynamic equations for V_l^m at the inner and outer most points are replaced with the boundary conditions $V_l^m = 0$ at $r = r_\mathrm{i}, r_\mathrm{o}$ (see the next section for a more detailed description of the handling of boundary conditions). The resulting matrix eigenvalue problem has been solved directly with a QR routine. Numerical approximations for p obtained in this manner had in general non-zero real parts. Eigenvalues occurred of course in complex conjugate pairs and real parts were distributed symmetrically with respect to $\mathrm{Re}\{p\} = 0$. Eigenvalues with positive real part potentially lead to instability of any time stepping scheme even at E different from zero. Table I, therefore, lists the eigenvalue with the largest real part for different resolutions. The numerical results corroborate the theoretical expectation. In order to reduce $\mathrm{Re}\{p\}$ to insignificant levels, the radial resolution needs to be large enough, and it needs to be the larger the more spherical harmonics are retained. Eigenvalues with $\mathrm{Re}\{p\} > 0$ always exist so that the spatial discretization described here will only allow stable time integration for $E \neq 0$. However, for any $E \neq 0$, the maximum of $\mathrm{Re}\{p\}$ can be reduced to harmless levels by increasing the radial resolution.

Table I. Eigenvalues p with the largest real part for $m = 1$, $r_\mathrm{i}/r_\mathrm{o} = 0.35$ computed at different resolutions n_r, L with the Eispack routines 'balance', 'elmhes' and 'hqr'

n_r	L	p
5	2	$10^{-16} + i \cdot 1$
5	8	$6.050 \times 10^{-2} + i \cdot 0.134$
9	4	$9.351 \times 10^{-9} + i \cdot 0.820$
9	6	$3.024 \times 10^{-3} + i \cdot 1.392$
9	8	$7.807 \times 10^{-3} + i \cdot 1.023$
9	16	$7.081 \times 10^{-2} + i \cdot 0.671$
7	8	$1.263 \times 10^{-8} + i \cdot 0.400$
17	10	$3.978 \times 10^{-8} + i \cdot 0.282$
17	12	$4.950 \times 10^{-4} + i \cdot 1.534$
17	16	$3.995 \times 10^{-3} + i \cdot 0.237$

3. TEMPORAL DISCRETIZATION

In order to avoid stringent CFL restrictions, the diffusion term is treated implicitly. This is feasible because the Laplacian decouples in l, m and the poloidal and toroidal scalars, resulting in systems of linear equations of manageable size. All other terms (the right-hand-sides of (6)) need to be integrated explicitly. Adams–Bashforth schemes of second- and third-order have been used for the explicit part. A Euler step is employed for starting up a run. Three choices for the implicit step are discussed below: Crank–Nicolson, implicit Euler and an integrating factor technique.

At the beginning of each time step all fields and their first- and second-radial derivatives are given in r,l,m-space. $\boldsymbol{u}$ and $\nabla \times \boldsymbol{u}$ are calculated from the poloidal and toroidal fields, transformed into r, θ, φ space where the non-linear terms are evaluated, which are then transformed back into r,l,m-space to yield the right-hand-sides of (6). Dealiasing in the angular variables can be performed during this last transformation. As can be deduced from [3], dealiasing is possible with the standard 3/2 rule in both θ- and φ-directions. The azimuthal co-ordinate is transformed with an FFT. The l to θ transform requires adding associated Legendre functions and the inverse transform consists in a Gauss quadrature. Both operations are expressed as matrix multiplications with matrices precomputed during initialization.

During the implicit time step a set of n_r linear equations needs to be solved for every pair l, m. The coefficients in these equations are independent of m. Let us first consider the equation for the toroidal scalar (6b). The discretized equations are formulated such that the updated toroidal field is obtained in n,l,m-space, where the radial derivatives required for the next time step can be conveniently computed. For an implicit Euler time step of size h, the coefficient matrices $\boldsymbol{C}^l$ are constructed such that

$$\sum_{j=1}^{n_r} C^l_{n,j} w^m_{l,j} = \sum_{j=1}^{n_r} w^m_{l,j} \left[T_{j-1}(x_n) - hE\left(\frac{\partial^2}{\partial r^2} + \frac{4}{r}\frac{\partial}{\partial r} + \frac{2-l(l+1)}{r^2} \right) T_{j-1}(x_n) \right]$$
$$n = 2, \ldots, n_r - 1, \quad l = 1, \ldots, L. \tag{14}$$

For a Crank–Nicolson step, h is replaced by $h/2$. In practice, the matrix elements of $\boldsymbol{C}^l$ are computed by looping the vector $(w^m_{l,1}, \ldots, w^m_{l,n_r})^T$ through all unit vectors and computing each time the right-hand-side of (14) with derivative routines that are necessary for the main program anyway. This allows filling $\boldsymbol{C}^l$ column by column. Boundary conditions are enforced by using the equations corresponding to the boundary points:

$$C^l_{1,j} = 1, \quad C^l_{n_r,j} = (-1)^{j-1}, \quad j = 1, \ldots, n_r, \quad l = 1, \ldots, L. \tag{15}$$

Note that the x_n are indexed such that $x_1 = 1$ and $x_{n_r} = -1$. The $\boldsymbol{C}^l$ are computed and inverted during initialization. If $\boldsymbol{w}^m_l$ denotes the n_r-dimensional vectors containing the elements $w^m_{l,n}$, $n = 1, \ldots, n_r$, $\boldsymbol{W}^m_l(t)$ the vectors containing $W^m_l(r_n, t)$, $n = 1, \ldots, n_r$, and $\boldsymbol{N}^m_l$ the n_r-dimensional vectors containing the right-hand-sides of (6b) evaluated at the collocation points, modified such that $N^m_{l,1} = N^m_{l,n_r} = 0$, then the solution of

$$\boldsymbol{C}^l \boldsymbol{w}^m_l(t+h) = \boldsymbol{W}^m_l(t) + \frac{h}{2}(3\boldsymbol{N}^m_l(t) - \boldsymbol{N}^m_l(t-h)), \quad l = 1, \ldots, L \tag{16}$$

yields the toroidal scalar at time $t+h$ in terms of quantities known from previous time steps using second-order Adams–Bashforth for the explicit part. In a Crank–Nicolson step, the vector containing

$$\frac{h}{2}E\left(\frac{\partial^2}{\partial r^2}+\frac{4}{r}\frac{\partial}{\partial r}+\frac{2-l(l+1)}{r^2}\right)W_l^m(r_n,t)$$

evaluated at the inner collocation points and set to zero at the boundaries needs to be added to the right-hand-side.

The poloidal equation (6a) is more complicated in that it is fourth-order and involves two boundary conditions at each boundary. A straightforward extension of the above method takes these extra boundary conditions into account by sacrificing the dynamic equations at two more collocation points, typically those next to the boundaries. The poloidal time step is then the direct analog of (16) with the $\boldsymbol{C}^l$ replaced with matrices $\boldsymbol{C}'^l$ defined by

$$\sum_{j=1}^{n_r} C'^l_{n,j}v^m_{l,j}=\sum_{j=1}^{n_r} v^m_{l,j}[\mathscr{D}_l T_{j-1}(x_n)-hE\mathscr{D}_l^2 T_{j-1}(x_n)],\quad n=3,\ldots,n_r-2,\quad l=1,\ldots,L, \tag{17a}$$

$$C'^l_{1,j}=1,\qquad C'^l_{n_r,j}=(-1)^{j-1},\quad j=1,\ldots,n_r, \tag{17b}$$

$$C'^l_{2,j}=(j-1)^2,\qquad C'^l_{n_r-1,j}=(-1)^j(j-1)^2,\quad j=1,\ldots,n_r. \tag{17c}$$

This practice wastes collocation points and integrating factor techniques are not readily implemented. An alternative uses a variant of Green's function or influence matrix method [1]. Explicit formulas will be given for an implicit Euler step, the extension to Crank–Nicolson is again straightforward.

The principle of the method is best introduced in terms of continuous functions. During initialization, discrete approximations are computed for the functions $f_{1,l}(r)$, $f_{2,l}(r)$, $g_{1,l}(r,t)$, $g_{2,l}(r,t)$, which are solutions of

$$\mathscr{D}_l f_{1,l}=0,\qquad f_{1,l}(r_\mathrm{i})=1,\qquad f_{1,l}(r_\mathrm{o})=0, \tag{18a}$$

$$\mathscr{D}_l f_{2,l}=0,\qquad f_{2,l}(r_\mathrm{i})=0,\qquad f_{2,l}(r_\mathrm{o})=1, \tag{18b}$$

$$\frac{\partial}{\partial t}g_{j,l}-E\mathscr{D}_l g_{j,l}=f_{j,l},\qquad g_{j,l}(r_\mathrm{i},t)=g_{j,l}(r_\mathrm{o},t)=0,\qquad g_{j,l}(r,t=0)=0,\quad j=1,2. \tag{18c}$$

At every single time step, the following equations are solved for $f^m_{0,l}$ and $g^m_{0,l}$:

$$\mathscr{D}_l f^m_{0,l}=\frac{r}{l(l+1)}[\hat{\boldsymbol{r}}\cdot\nabla\times\nabla\times\{\boldsymbol{\Omega}'\times\boldsymbol{u}\}]^m_l,\qquad f^m_{0,l}(r_\mathrm{i})=f^m_{0,l}(r_\mathrm{o})=0, \tag{19a}$$

$$\frac{\partial}{\partial t}g^m_{0,l}-E\mathscr{D}_l g^m_{0,l}=f^m_{0,l},\qquad g^m_{0,l}(r_\mathrm{i},t)=g^m_{0,l}(r_\mathrm{o},t)=0,\qquad g^m_{0,l}(r,t_n)=V^m_l(r,t_n), \tag{19b}$$

where t_n is the time at the beginning of the current time step. The poloidal field is finally updated by:

$$V^m_l(r,t_{n+1})=g^m_{0,l}(r,t_n+h)+a^m_{1,l}g^m_{1,l}(r,h)+a^m_{2,l}g^m_{2,l}(r,h). \tag{20}$$

V^m_l is zero by construction at the boundaries and the coefficients $a^m_{1,l}$ and $a^m_{2,l}$ are uniquely determined by the second boundary condition on V^m_l.

In order to discretize the method two sets of matrices, $\boldsymbol{P}^l$ and $\boldsymbol{M}^l$, are necessary. In connection with the Poisson inversions ((18a), (18b) and (19a)) we need $\boldsymbol{P}^l$ such that for arbitrary $f(r)$ and its Chebychev coefficients $\tilde{f}_j$ with $f(r_n)=\Sigma_{j=1}^{n_r}\tilde{f}_j T_{j-1}(x_n)$, $n=1,\ldots,n_r$, the following property holds:

$$\sum_{j=1}^{n_r} P^l_{n,j} f(r_j) = \sum_{j=1}^{n_r} \tilde{f}_j \mathscr{D}_l T_{j-1}(x_n), \quad n = 2, \ldots, n_r - 1, \quad P^l_{1,j} = \delta_{1,j}, \quad P^l_{n_r,j} = \delta_{n_r,j},$$
$$j = 1, \ldots, n_r, \quad l = 1, \ldots, L. \tag{21}$$

For the actual time step we need in analogy with (14), matrices $\boldsymbol{M}^l$ with the property

$$\sum_{j=1}^{n_r} M^l_{n,j} \tilde{f}_j = \sum_{j=1}^{n_r} \tilde{f}_j [T_{j-1}(x_n) - hE\mathscr{D}_l T_{j-1}(x_n)], \quad n = 2, \ldots, n_r - 1, \quad M^l_{1,j} = 1,$$
$$M^l_{n_r,j} = (-1)^{j-1}, \quad j = 1, \ldots, n_r, \quad l = 1, \ldots, L, \tag{22}$$

for any $\tilde{f}_j$.

The discrete analogs of (18a) and (18b) are now:

$$\boldsymbol{P}^l(f_{1,l}(r_1), \ldots, f_{1,l}(r_{n_r}))^T = (0, \ldots, 0, 1)^T, \tag{23a}$$

$$\boldsymbol{P}^l(f_{2,l}(r_1), \ldots, f_{2,l}(r_{n_r}))^T = (1, 0, \ldots, 0)^T. \tag{23b}$$

(18c) becomes

$$\boldsymbol{M}^l(\tilde{g}_{j,l,1}, \ldots, \tilde{g}_{j,l,n_r})^T = (0, f_{j,l}(r_2), \ldots, f_{j,l}(r_{n_r-1}), 0)^T, \quad j = 1, 2, \tag{24}$$

where a tilde again denotes Chebychev coefficients. The extension to (19a) and (19b) as well as to the Crank–Nicolson step is obvious.

It will now be argued that Crank–Nicolson (CN) can be a dangerous method in some circumstances. There is the well-known fact that the implicit Euler step 'damps small scales better' than CN. CN does not necessarily preserve the hierarchy of damping rates, which is disturbing for very stiff equations. In particular, when looking for the most slowly decaying mode of a system, CN may pick the wrong one. As a simple example, consider the model equation

$$\frac{\mathrm{d}}{\mathrm{d}t} y(t) = \lambda y(t) \tag{25}$$

for $y(t)$ with the growth rate λ. The value of y at two instants separated by the time lapse h is exactly determined by $y_{n+1} = \xi y_n = \mathrm{e}^{\lambda h} y_n$. If (25) is discretized with CN and implicit Euler steps of step size h, one obtains respectively ξ_{CN} and ξ_{E} for the ratio of y at two successive time steps:

$$\xi_{CN} = \frac{1 + \lambda h/2}{1 - \lambda h/2}, \tag{26a}$$

$$\xi_{\mathrm{E}} = \frac{1}{1 - \lambda h}. \tag{26b}$$

Figure 1 compares these damping rates. It is seen that for $\lambda h = -2$, CN sets y to zero after just one time step. For $\lambda h < -2$, the sign of y alternates between successive time steps and the absolute value of y decays more slowly for a larger $|\lambda|$! In this parameter range, the implicit Euler step, though first-order, is closer to the exact solution than CN. Transposed to a stiff system of equations, this means that very rapidly decaying modes are more accurately reproduced by the implicit Euler step than by CN.

As a simple application to the spherical code, let us consider the solutions $\psi(r, t)$ of the equation

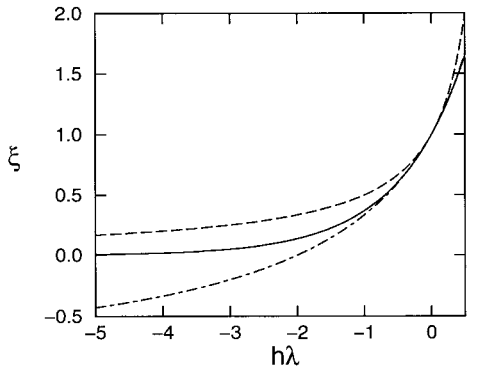

Figure 1. Ratio ξ of the solution of (25) at two successive time steps separated by the time h if (25) is integrated with the implicit Euler (dashed) or the Crank–Nicolson (dot dashed) method. The solid line shows the exact value of ξ.

$$\frac{\partial}{\partial t}\psi(r,t)-\left(\frac{\partial^2}{\partial r^2}+\frac{4}{r}\frac{\partial}{\partial r}+\frac{2-l(l+1)}{r^2}\right)\psi(r,t)=0, \qquad \psi(r_\mathrm{i},t)=\psi(r_\mathrm{o},t)=0, \tag{27}$$

which corresponds to the diffusive part of (6b). ψ should converge to a toroidal decay mode if (27) is integrated for long enough starting from arbitrary initial conditions. Figure 2 shows ψ for $l=1$ and $r_\mathrm{i}/r_\mathrm{o}=0.35$ at $t=1$ obtained with a resolution of $n_r=65$ and different time stepping methods starting from $\psi(r,0)=\sin\pi(r-r_\mathrm{i})$. The time step was $h=0.01$, whereas the decay time of the relevant decay mode is 0.084. The integrating factor technique to be discussed below yields an exact temporal discretization of (27). It is seen that CN approximates well the desired solution throughout most of the computational interval but develops unphysical oscillations near the boundaries. The implicit Euler step is overall less accurate but at least qualitatively correct (as concerns the number of nodes of the solution, for instance). Upon decreasing h, the oscillations in the CN solution gradually disappear and the implicit Euler solution becomes more accurate.

In the light of the discussion connected with (25), the oscillations are interpreted as being due to an eigenmode of (27), which does not decay fast enough in the CN scheme. The CN step is, therefore, to be used with caution in problems dealing with a system of modes with widely varying decay rates. Highly oscillatory modes that are insufficiently damped may of course also lead to instabilities if non-linear terms are included.

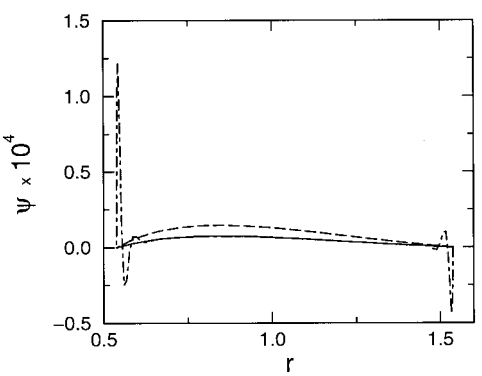

Figure 2. Solution ψ of (27) for the parameters given in the text obtained with the implicit Euler (dashed), Crank–Nicolson (dot dashed) and integrating factor (solid) techniques.

We are thus motivated to search for a method that integrates the diffusive part exactly in order to obtain accurate damping rates. A suitable integrating factor technique will now be presented. Let us once again consider the toroidal problem first:

$$\frac{\partial}{\partial t} W_l^m + \mathscr{L}_l W_l^m = F_l^m(r, t), \qquad W_l^m(r_\mathrm{i}) = W_l^m(r_\mathrm{o}) = 0, \tag{28}$$

where

$$\mathscr{L}_l = E\left(\frac{\partial^2}{\partial r^2} + \frac{4}{r}\frac{\partial}{\partial r} + \frac{2 - l(l+1)}{r^2}\right)$$

and $F_l^m(r, t)$ stands for the right-hand-side of (6b). The indices l and m are unnecessary in the following and will be omitted. Equation (28) can be formally rewritten as $\partial(\mathrm{e}^{\mathscr{L}t}W)/\partial t = \mathrm{e}^{\mathscr{L}t}F$. Because W is always zero at the boundaries, the action of $\mathscr{L}$ at the $n_r - 2$ interior collocation points can be described by the $(n_r - 2)^2$ matrix $\boldsymbol{L}$ in a manner analogous to (21):

$$\sum_{j=2}^{n_r-1} L_{n,j}^l f(r_j) = \sum_{j=1}^{n_r} \tilde{f}_j \mathscr{L} T_{j-1}(x_n), \quad n = 2, \ldots, n_r - 1 \tag{29}$$

for arbitrary functions f. Integrating the spatially discretized dynamic equations from time t_n to $t_{n+1} = t_{n+h}$ yields

$$\exp(\boldsymbol{L}t_{n+1})\boldsymbol{\omega}_{n+1} - \exp(\boldsymbol{L}t_n)\boldsymbol{\omega}_n = \int_{t_n}^{t_{n+1}} \exp(\boldsymbol{L}t')\boldsymbol{F}(t')\,\mathrm{d}t', \tag{30}$$

where the $(n_r - 2)$-dimensional vectors containing the values of the toroidal scalar and F at the interior collocation points at time t_n are denoted by $\boldsymbol{\omega}_n$ and $\boldsymbol{F}(t_n)$ respectively. The exponentials can be computed after diagonalization of $\boldsymbol{L}$:

$$\exp(\boldsymbol{L}t) = \boldsymbol{T}\exp(\boldsymbol{T}^{-1}\boldsymbol{L}\boldsymbol{T}t)\boldsymbol{T}^{-1}, \tag{31}$$

where $\boldsymbol{T}^{-1}\boldsymbol{L}\boldsymbol{T}$ is diagonal and $\boldsymbol{T}$ contains the eigenvectors of $\boldsymbol{L}$ in its columns. Sturm–Liouville theory tells us that the eigenfunctions of $\mathscr{L}$ form a complete set of functions. It is not guaranteed that this property transposes to $\boldsymbol{L}$, the Chebychev discretization of $\mathscr{L}$. Numerical tests in double precision arithmetic have shown however that $\boldsymbol{T}^{-1}\boldsymbol{T}$ differs from the identity matrix by no more than 10^{-16} in each element for 63^2 matrices when $\boldsymbol{T}$ is computed with QR and $\boldsymbol{T}^{-1}$ is obtained after LU decomposition, indicating that $\boldsymbol{T}$ is well-conditioned.

The integral on the right-hand-side of (30) is now approximated by discretizing $\boldsymbol{F}$ according to the second order Adams–Bashforth scheme:

$$\begin{aligned}\int_{t_n}^{t_{n+1}} \exp(\boldsymbol{L}t')\boldsymbol{F}(t')\,\mathrm{d}t' &\approx \int_{t_n}^{t_{n+1}} \exp(\boldsymbol{L}t')\,\mathrm{d}t' \frac{h}{2}[3\boldsymbol{F}(t_n) - \boldsymbol{F}(t_{n-1})] \\ &= (\exp(\boldsymbol{L}t_{n+1}) - \exp(\boldsymbol{L}t_n))\boldsymbol{\Lambda}\frac{h}{2}[3\boldsymbol{F}(t_n) - \boldsymbol{F}(t_{n-1})],\end{aligned} \tag{32}$$

where $\boldsymbol{\Lambda} = \boldsymbol{T}\,\mathrm{diag}\{\lambda_i\}\boldsymbol{T}^{-1}$ and λ_i are the eigenvalues of $\boldsymbol{L}$. The updated toroidal scalar is finally given by:

$$\boldsymbol{\omega}_{n+1} = \exp(-\boldsymbol{L}h)(\boldsymbol{\omega}_n - \tilde{\boldsymbol{F}}) + \tilde{\boldsymbol{F}}; \quad \boldsymbol{F} = \boldsymbol{\Lambda}\frac{h}{2}[3\boldsymbol{F}(t_n) - \boldsymbol{F}(t_{n-1})]. \tag{33}$$

Two matrix multiplications are thus required, involving the matrices $\boldsymbol{\Lambda}$ and $\exp(-\boldsymbol{L}h)$, which can be precomputed during initialization. Two cosine transforms are necessary when computing the radial derivatives for the next time step.

Table II. The kinetic energy E_{kin} computed for $r_i/r_o = 0.35$, $\alpha = 23.5°$, $\Omega = -10^{-3}$, $E = 10^{-4}$ at a resolution of $n_r = 65$, $L = 64$ with 12 longitudinal grid points, time step h and three different methods: implicit Euler step using four collocation points to enforce the boundary conditions on the poloidal field (IE4), implicit Euler step using the Green's function method for the poloidal field (IEG), and the integrating factor method (IF)[a]

Method	h	$E_{kin} \times 10^3$
IE4	0.1	3.286
IEG	0.1	3.285
IF	0.1	3.256
IE4	0.03	3.45025
IEG	0.03	3.45027
IF	0.03	3.4514
IE4	0.01	3.45983
IF	0.01	3.46029

[a] Non-linear and Coriolis terms were treated with second-order Adams–Bashforth and the precessional forcing term with Crank–Nicolson. The non-linear products were dealiased with the 3/2 rule in the azimuthal direction. The simulations were started from rest and integrated until time $t = 900$. IF with $h = 0.01$ is expected to yield the most accurate result.

No essential changes are necessary to apply the integrating factor technique to the poloidal equation if the influence matrix method is used. In this case, time steps occur only in (18c) and (19b) with boundary conditions that the solution be zero at the boundaries. The above formulas can thus directly be used. It is, however, considerably more involved to design an efficient integrating factor technique for the poloidal field if one insists on imposing the boundary conditions by sacrificing a total of four collocation points. One reason is that the remaining dynamic equations are not any more described by a square matrix one could formally exponentiate.

With the implementations used by the author, the CPU time requirements for (i) a CN (or implicit Euler) method using four collocation points to enforce the boundary conditions for the poloidal field, (ii) a CN step using the influence matrix method, and (iii) the integrating factor technique stand in the ratio 1:1.23:1.37 for $n_r = 65$, $L = 64$.

4. CONCLUSION

Several time stepping methods have been presented in this paper for the integration of the incompressible Navier–Stokes equation in a spherical shell. Examples of numerical results for different problems obtained at various stages of development of the code can be found in the literature [7–10]. The Crank–Nicolson step has been applied successfully in many cases despite its shortcomings. The implicit Euler step may procure higher 'fidelity' by yielding qualitatively correct answers as in the above example of the decaying flow. This time step is, however, only first-order in time and the integrating factor technique is preferred for accurate computations.

Precession driven flows are a case in point. One way to look at precessional flows is to think of the flow field as a sum of inertial modes (which exist in the purely rotating container) excited by precession. Modes in resonance with precessional forcing acquire the largest amplitude. These are mainly an $m = 1$ mode (the 'spin-over' mode) so that an accurate spectral computation gets away with only a few azimuthal modes corresponding to few grid points in

longitude. On the other hand, it is important to make sure that some modes do not accumulate an unrealistic amount of energy as could happen with the Crank–Nicolson step. A mode by mode comparison of the amplitudes obtained with different time marching methods is thus recommendable.

At large E, diffusion dominates and the Crank–Nicolson step is indeed an unacceptable method; the same phenomenon is observed as in the decay problem (27). At small E, the primary balance of forces does not involve diffusion, and the choice of the implicit time step becomes less and less important. Even the fact that the implicit Euler step is only first-order becomes irrelevant. The limit imposed on the time step by the CFL condition becomes small compared with the diffusion time scale so that diffusion is accurately treated and computational precision is limited by the explicit part of the time step. Table II gives a specific numerical example. A further distinction is whether Green's functions are used or not. These are definitely useful to formulate the integrating factor technique but do not provide a clear advantage for the other methods.

In summary, the integrating factor technique is the most universal and can be used in all cases, but simpler and somewhat faster executing methods may suffice in flows in which viscous forces are overwhelmed by other forces.

REFERENCES

1. C. Canuto, M.Y. Hussaini, A. Quarteroni and T.A. Zang, *Spectral Methods in Fluid Dynamics*, Springer, New York, 1988.
2. S.A. Orszag, 'Fourier series on spheres', *Month. Weather Rev.*, **102**, 56–75 (1974).
3. R.E. Young, 'Finite amplitude thermal convection in a spherical shell', *J. Fluid Mech.*, **63**, 695–721 (1974).
4. G.A. Glatzmaier, 'Numerical simulations of stellar convective dynamos. I. The model and method', *J. Comp. Phys.*, **55**, 461–484 (1984).
5. G. Backus, 'A class of self-sustaining dissipative spherical dynamos', *Ann. Phys.*, **4**, 372–447 (1958).
6. G. Dumas and A. Leonard, 'A divergence-free spectral expansions method for three-dimensional flows in spherical-gap geometries', *J. Comp. Phys.*, **111**, 205–219 (1994).
7. A. Tilgner, 'High Rayleigh number convection in spherical shells', *Phys. Rev. E*, **53**, 4847–4851 (1996).
8. A. Tilgner and F.H. Busse, 'Finite-amplitude convection in rotating spherical fluid shells', *J. Fluid Mech.*, **332**, 359–376 (1997).
9. A. Tilgner, 'A kinematic dynamo with a small scale velocity field', *Phys. Lett. A*, **226**, 75–79 (1997).
10. A. Tilgner, 'Magneto-hydrodynamic flow in precessing spherical shells', *J. Fluid Mech.*, **379**, 303–318 (1999).
11. W.V.R. Malkus, 'Precession of the earth as the cause of geomagnetism', *Science*, **160**, 259–264 (1968).
12. H.P. Greenspan, *The Theory of Rotating Fluids*, Cambridge University Press, Cambridge, 1968.

